Ultrasonics 83 (2018) 68–79

Contents lists available at ScienceDirect

Ultrasonics

journal homepage: www.elsevier.com/locate/ultras

Characterization of nanoparticles doped composites using ultrasound

Alberto Rodríguez-Martínez [a,*], Miguel Ángel de la Casa-Lillo [b], Linas Svilainis [c], Tomás E. Gomez Álvarez-Arenas [d]

[a] Communications Engineering Dept., UMH, Avda. Universidad S/N, 03202 Elche, Spain
[b] Bioengineering Institute, UMH, Avda. Universidad S/N, 03202 Elche, Spain
[c] Electronic Engineering Dept., KTU, Studentu St. 48, LT-51367 Kaunas, Lithuania
[d] Instituto de Acústica, CSIC, 28006 Madrid, Spain

ARTICLE INFO

Article history:
Received 16 February 2017
Received in revised form 29 April 2017
Accepted 19 June 2017
Available online 20 June 2017

Keywords:
Nanoparticles
Graphene
Composites
Elastic constants
Mechanical characterization

ABSTRACT

The aim of this work is the non-destructive automatic mechanical characterization of nanoparticles doped composites using ultrasound in order to understand and control the dispersion of the dopant nanoparticles in the final product. We present a method which is able to measure the elastic constants of composites (Youngs, Bulk, Shear Modulus and Poissons ratio), in addition to other parameters as density, sound velocity and thickness, providing information of the nanoparticles dispersion in the samples. All results are obtained with a single ultrasonic measure at each point of the samples' surface in an immersion setup with both pulse-echo and through-transmission measurements simultaneously, obtaining detailed information for all the samples' surface in a XY scanning. All the analysis is performed automatically, that is, no manual correction or adjustment is needed at any stage of the process. To validate the results, a polyester based resin has been analyzed with different concentrations of graphene nanoparticles as dopant. The method has shown to be very accurate and reliable. The resolution of the values obtained for the elastic constants is limited by the resolution in the velocities measurements, for which we have achieved a resolution in the order of cm/s, thus providing very accurate measurements of the elastic constants.

1. Introduction

Nowadays it is almost impossible to find an area in the industry in which composites are not used. From aircraft and aerospace industries to dental restorative composites we will find a wide set of applications: wind mills, containers, automotive and marine structures, chassis and hulls, helmets, glasses, wearables, etc. They can also be designed with specific physical or chemical properties, as photo-sensitivity, electromagnetic-sensitivity or thermo-sensitivity, that make them suitable for the design of sensors and actuators. Even ballistic protective layers of polymers can be easily applied to all of the above items. One of the pioneers and most successful uses of composites are those related to mechanic structures. Most of the structures developed nowadays share the same principle: a polymer matrix reinforced with fibers. The possible combinations extend to a wide variety of solutions, but mainly using either epoxy, vynilester or polyester resins reinforced with glass, carbon or aramide fibers, processed and formed in many different ways: Autoclave, Poltrusion, Resin Transfer Molding, etc. In the last few years, the revolution of nanotechnology has spread to the field of composites resulting in a new set of plastic and resin-based composites [1–5].

These nano-filled polymer composites are obtained adding nanoparticles to the polymer matrix to enhance its properties. It is easy to find hundreds of research works related to the use of nanomaterials and polymers [2,6–8], but it is very difficult to apply those in commercial products like aircrafting or boating industries. One of the reasons is that it is very difficult to integrate the nanomaterial (in the form of nanoparticles or nanotubes) in the manufacturing process, mainly due to two factors. On the one hand, the mixture in industrial volumes of the polymer matrix and the nanoparticles does not always result in a homogeneous product, which could be due to several factors, such as the integration of the nanoparticles in the local chemistry of the polymer chain [6,9–11], or simply the functionalization of the nanoparticles before the mixing [9,12]. On the other hand, even if the mixing is homogeneous, nanoparticles (especially in the case of nanofibers and nanotubes) tend to agglomerate around the fibers of the fabric used as reinforcement, impeding the correct diffusion of the

* Corresponding author.
E-mail addresses: arodriguezm@umh.es (A. Rodríguez-Martínez), mcasa@umh.es (M.Ángel de la Casa-Lillo), linas.svilainis@ktu.lt (L. Svilainis), t.gomez@csic.es (T.E. Gomez Álvarez-Arenas).

http://dx.doi.org/10.1016/j.ultras.2017.06.017
0041-624X/

mixture throughout the material. As a result, the homogeneity of the mechanical behavior in the final product is compromised, especially in the construction of large structures and surfaces, as windmills wings, boat hulls or containers.

Due to the above, it is essential to conduct a study to analyze the dispersion of nanoparticles in the final product. This can be done using the elastic moduli of the materials, closely related to their mechanical properties. Usually, this is made in the manufactures' laboratories using tensile stress tests, which provide information about the elasticity modulus. Unfortunately, these methods have some drawbacks that make them not suitable when the goal of the test is the analysis of nanoparticles dispersion within the samples, or in other words, how homogeneous is the mechanical behavior of the sample along its surface. These measurements provide an average of the specimen properties, but not information about the real dispersion of the nanoparticles. Furthermore, specimens crack in the weakest point, which could be due to an improper dispersion of nanoparticles in that particular point. To have an idea of the product behavior, it requires the analysis of a high number of specimens, and even then the result can be both inaccurate and ambiguous. Finally, these measurements are highly time consuming, require expensive equipment and trained personnel.

There are many other techniques that can be used, as Dynamic Mechanical Analysis (DMA) [12,13], Thermomechanical Analysis (TMA) [13], Thermal Gravimetric Analysis (TGA) [13,14], Atomic Force Microscopy (AFM) [15], UV–vis Absorption Spectra [15], Raman Spectra [15], IR Spectroscopy [14,17], Fourier Transform Infrared Spectroscopy (FT-IR) [13], X-ray Photoelectron Spectroscopy (XPS) [14], X-ray Diffraction (XRD) [11,14–17], Transmission Electron Microscopy (TEM) [11,13–16] and Scanning Electron Microscopy (SEM) [11,13,15]. Unfortunately, they all have serious shortcomings, including one or more of the following:

1. Required equipment is very expensive.
2. They require very specialized and trained technicians.
3. They provide information about the inner structure of the materials, but not about their mechanical properties.
4. They do not provide information locally, and/or only from the surface.
5. They required specific manipulation of the samples (which can affect the actual mechanical properties of the product) and/or additional facilities (thermal chambers, vacuum, etc.).
6. Results are difficult to interpret, and could even be biased by the samples manipulation required.

In conclusion, all those techniques are good, but do not allow whole sample inspection, sometimes use dangerous radiation, use complex equipment, are quiet expensive, and most relevant for our goal, they do not provide information about the distribution of the mechanical properties locally.

Using ultrasound it is possible to control the process in situ in the laboratory or in the manufacturer workshop, which is a qualitative advantage for the end product, plus it can result in the reduction of costs and production time. Ultrasonic techniques can provide the elastic constants of the materials as a function of the longitudinal and shear propagation velocities and the density of the samples. Several methods can be found for the accurate calculation of the velocities at any point in the material [18–20], but in the case of the density it is not so simple. Although there are numerous methods to obtain the density of solids in the laboratory (densitometer, pycnometer, etc.), these require additional laboratory equipment and preparation of the samples, and results may be inaccurate. On the other hand, there are the methods that use ultrasound, using the relationship between the acoustic impedance, propagation velocity and density. There are numerous well known techniques for obtaining these parameters [21–25], but they require complicated processes for correcting the diffraction due to the difference in the propagation path of each pulse as well as parallelism between surfaces.

In this work we present a simple and fast method to calculate all the parameters needed to obtain the elastic constants of doped resin samples produced in the laboratory, and therefore to estimate the dispersion of the nanoparticles within the sample. With this method, in a single measurement and at each point on the surface of the analyzed specimen, it calculates automatically the propagation velocities, the thickness and the density with high accuracy, and without the need of any prior knowledge about the samples besides its mass. It is automatic and does not need any specific calibration nor the action of the user except changing the samples between measurements.

The work is organized as follows. It starts in Section 2 with a short review of the mechanical properties of the materials to introduce the relation between elastic constants and sound velocity. Section 3 describes the method followed for the calculation of the ultrasonic parameters involved in the analysis. Section 4 describes the different set-ups designed for the experiments and the results obtained after the analysis of the samples. Finally, conclusions will be summarized and discussed in Section 5.

2. Review of the mechanical properties of the materials

2.1. Stress, strain and stiffness

The elastic properties of solids are key properties for the design of mechanically loaded components [2,26–28]. Specially, the elastic modulus and Poissons ratio, which describe the elastic behavior of isotropic materials. The elastic moduli measure the resistance opposed by a material to being deformed elastically, and is measured as the ratio between the stress applied and the resulting strain. The stress is the force causing the deformation divided by the area to which the force is applied and it is measured in Pascals, and strain is the ratio of the change in some length parameter and the original value of the length parameter, therefore dimensionless.

The state of stress at an arbitrary point P in a structure depends on the orientation of the applied force F acting on P and the orientation of the reference plane with respect to a reference coordinate system. If the point P under analysis is considered as an infinitesimal cube, the stress acting on each of the six sides of the cube can be resolved into components normal to the face and within it, as shown in Fig. 1, in which a plane oriented normal to an axes i is called the i-plane.

A stress σ_{ij} is defined as acting on the i-plane and being oriented in the j direction. Components of the stress tensor perpendicular to the considered plane are denoted as normal stress (σ_{ii}), while stress components acting in the same plane are called shear stress (σ_{ij}), resulting in six shear and three normal stress components

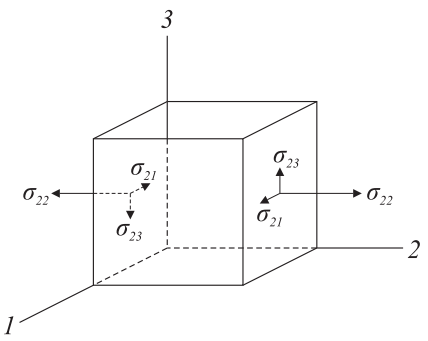

Fig. 1. Example of stress components acting on plane 2.

acting on the cube. If the medium is in static equilibrium the sum of all stress components and the total moment is zero, so that $\sigma_{ij} = \sigma_{ji}$. Thus, the stress tensor σ_{ij} completely describes the state of stress at any point:

$$\sigma_{ij} = \begin{pmatrix} \sigma_{1,1} & \sigma_{1,2} & \sigma_{1,3} \\ \sigma_{2,1} & \sigma_{2,2} & \sigma_{2,3} \\ \sigma_{3,1} & \sigma_{3,2} & \sigma_{3,3} \end{pmatrix} \tag{1}$$

On the other hand, the strain at point P is determined by the strain tensor (ε_{ij}), assuming the deformations to be sufficiently small:

$$\varepsilon_{ij} = \begin{pmatrix} \varepsilon_{1,1} & \varepsilon_{1,2} & \varepsilon_{1,3} \\ \varepsilon_{2,1} & \varepsilon_{2,2} & \varepsilon_{2,3} \\ \varepsilon_{3,1} & \varepsilon_{3,2} & \varepsilon_{3,3} \end{pmatrix} \tag{2}$$

The elements of the strain tensor with repeating index are denoted as normal strain, all others as shear strain, and just as with the stress, the strain tensor has six independent components, so that $\varepsilon_{ij} = \varepsilon_{ji}$.

In elastic mediums, that is, those in which the strain is assumed to be sufficient small that stress and strain depend linearly on each other, the relation between stress and strain is described by Hooke's Law, which can be written as:

$$\sigma_{ij} = C_{ijkl} \cdot \varepsilon_{kl}, \quad i,j,k,l = 1,2,3 \tag{3}$$

where C_{ijkl} is called the stiffness tensor composed of 81 elements that link the deformation of a medium to the applied stress. Hooke's law can be remarkably simplified in the case of isotropic media. Taking into account that stress components are linearly dependent upon the corresponding strain components, that the stress and strain tensors are symmetric and that there is only a unique strain energy potential, the number of independent elements of the stiffness tensor reduces to 21.

2.2. Elastic constants of isotropic media

In this work we are considering only simple composites formed from resins doped with nanoparticles, in which we assume as starting hypothesis that the distribution of the nanoparticles is random and locally homogeneous, therefore we can assume that, locally, the material behaves in an isotropic way. If this is the case, the material has only two independent elastic moduli, called the Lame constants λ, and μ, and the elastic properties at any point are independent of the direction. The Lame constants are related to the stiffness tensor by the following expression [28,29]:

$$C_{ijkl} = \left(\lambda\delta_{ij}\delta_{kl} + \mu\left(\delta_{ik}\delta_{jl} + \delta_{il}\delta_{jk}\right)\right) \cdot \varepsilon_{kl}, \quad i,j,k,l = 1,2,3 \tag{4}$$

where δ_{ij} is the Kronecker delta function:

$$\delta_{ij} = \begin{cases} 1 & i = j \\ 0 & i \neq j \end{cases} \tag{5}$$

On the other hand, the stiffness tensor of isotropic media in Voigt notation can be written as:

$$\varepsilon_{ij} = \begin{bmatrix} C_{11} & C_{12} & C_{13} & & & \\ C_{21} & C_{22} & C_{23} & & & \\ C_{31} & C_{32} & C_{33} & & & \\ & & & C_{55} & & \\ & & & & C_{55} & \\ & & & & & C_{55} \end{bmatrix} \tag{6}$$

with

$$C_{11} = C_{33} - 2C_{55} \qquad C_{55} = \mu \qquad C_{33} = K + \frac{4}{3}\mu \tag{7}$$

where K is the Bulk Modulus.

Using the above relations, some specific elastic parameters are defined from the stiffness tensor that are used to describe the elastic behavior of the materials. Such parameters are the Bulk modulus, the Shear modulus, the Young's modulus and the Poisson's Ratio.

The Bulk modulus (K), also called incompressibility, is defined as the ratio of an applied isostatic stress to the fractional volumetric change:

$$K = \frac{1}{3}\frac{\sigma_{ii}}{\varepsilon_{ii}} \tag{8}$$

The Shear modulus (μ) is a measure of resistance to shear stress:

$$\mu = \frac{1}{2}\frac{\sigma_{ij}}{\varepsilon_{ij}}, \quad i \neq j \tag{9}$$

The Young's modulus (E), relates the stress to the resulting strain in the same direction:

$$E = \frac{\sigma_{ii}}{\varepsilon_{ii}} \tag{10}$$

Finally, the Poisson's ratio (v), is also defined for a uniaxial stress state and relates the lateral strain (j-direction) to axial strain (i-direction). In contrast to the other elastic parameters which have physical units of pressure (Pascals), the Poisson's ratio is dimensionless, and it is defined as:

$$v = -\frac{\varepsilon_{jj}}{\varepsilon_{ii}} \tag{11}$$

2.3. Plane waves in isotropic media

In the case of ultrasonic wave propagation, when the ultrasonic wavelength is much greater than the size of the nanoparticles, isotropic assumptions are quite valid. Two types of bulk waves can propagate in isotropic solids, longitudinal and shear waves. Longitudinal waves produce a displacement of the material particles in the same direction of propagation. This displacement is therefore associated with normal stress. On the other hand, shear waves produce a displacement of the particles on a perpendicular plane to the direction of propagation. In the latter case, the displacements are associated with shear stresses [30–33].

An analytical description of plane waves in arbitrary anisotropic media can be derived using the elastodynamic relations between motion, stress and strain [28,33,34]. According to the equation of motion given by Newton's second law, which relates the stress acting on a point in a solid with the displacement of a particle in the i-direction:

$$\rho\frac{\partial^2 u_i}{\partial t^2} = \nabla\sigma_{ij,j} \tag{12}$$

where ρ is the density of the material, u_i the displacement of the particle in the i-direction, t is time and $\sigma_{ij,j}$ is the stress tensor resulting from the applied force in the j-direction, and ∇ denotes the gradient operator. If we introduce in (12) the relation between stress, strain and the stiffness tensor given by the Hookes law given by (3), we can write:

$$\rho\frac{\partial^2 u_i}{\partial t^2} = C_{ijkl} \cdot \nabla\varepsilon_{kl,j} \tag{13}$$

On the other hand, in isotropic media, the elastic strain can be given as a function of the gradient of the displacement by:

$$\varepsilon_{kl,j} = \frac{1}{2}\left(\nabla u_{k,l} + \nabla u_{l,k}\right) \tag{14}$$

so that (13) can be rewritten as:

$$\rho\frac{\partial^2 u_i}{\partial t^2}=\frac{1}{2}C_{ijkl}\cdot\left(\Delta u_{k,jl}+\Delta u_{l,jk}\right) \tag{15}$$

where Δ denotes the Laplacian operator. Note that in tensor notation, repeated indexes can be swapped without changing the equation, so that:

$$\rho\frac{\partial^2 u_i}{\partial t^2}=C_{ijkl}\cdot\Delta u_{k,jl} \tag{16}$$

which is the so called Cauchy's law of motion, a solution that can be assumed to take the form of a plane wave. In these sort of waves, the particle displacement u_i is given in a harmonic plane wave representation as a function of distance x and time t:

$$u(x,t)=A\cos\left(kx-\omega t\right)=Ae^{-j(kx-\omega t)} \tag{17}$$

where A is the amplitude of the wave, k is the wave number and ω the angular frequency. For a 3-dimensional wave in tensor notation, the displacement in direction i can be finally written as:

$$u_i=Ap_ie^{-j(k_ix_i-\omega t)} \tag{18}$$

where and p_i is the polarization vector given by:

$$p_i=\frac{u_i}{\sqrt{u_iu_j}} \tag{19}$$

and k_i is the wave vector given by $k_i=k\cdot n_i$, with n_i representing the wave propagation direction. Note that as the wave number relates the angular frequency ω and the wave velocity c, the wave vector can be written as:

$$k_i=\frac{\omega}{c}n_i \tag{20}$$

If we continue with the Cauchy's law of motion, differentiating u_i twice respect to time yields to:

$$\frac{\partial^2 u_i}{\partial t^2}=-\omega^2Ap_ie^{-j(kx-\omega t)}=-\omega^2u_i \tag{21}$$

and the Laplacian of $u_{k,jl}$ yields to:

$$\Delta u_{k,jl}=-k_jk_lu_k=-k^2n_jn_lu_k \tag{22}$$

Therefore, Cauchy's law in (16) can be rewritten as:

$$\rho\omega^2u_i=C_{ijkl}\cdot k^2n_jn_lu_k \tag{23}$$

and using the value of the wave number given in (21) we finally arrive to:

$$\rho c^2u_i=C_{ijkl}n_jn_lu_k \tag{24}$$

This equation can be rearranged in tensor notation to derive the so called Christoffels equation [28,29,32]:

$$\left[\rho c^2\delta_{ik}-C_{ijkl}n_jn_l\right]\left[u_k\right]=0 \tag{25}$$

In an isotropic media, for any direction δ_{ik}, the solution of (25) yields to two possible values for the velocity c. Note that when the polarization vector p_i is parallel to the propagation direction the wave is pure longitudinal, thus leading to the longitudinal velocity c_L. In the same way, the wave will be pure shear when the propagation direction is perpendicular to the waveform, thus leading to the shear velocity c_S. Therefore, for $k=i$ and $i=j$, and using Voigt notation for the stiffness matrix, we have the longitudinal velocity:

$$\rho c_l^2-C_{11}=0\Rightarrow c_l=\sqrt{\frac{C_{11}}{\rho}} \tag{26}$$

On the other hand, for $k=i$ and $i\neq j$, and using Voight notation for the stiffness matrix, we have the shear velocity:

$$\rho c_s^2-C_{55}=0\Rightarrow c_s=\sqrt{\frac{C_{55}}{\rho}} \tag{27}$$

Finally, using (8)–(11) in (26) and (27), the elastics constants of the material (Shear modulus, Young's modulus, Bulk modulus and Poisson's ratio respectively) can be written as a function of the density, the longitudinal velocity and the shear velocity of the material as:

$$\mu=\rho c_s^2 \tag{28}$$

$$E=\rho\frac{c_s^2\left(3c_l^2-4c_s^2\right)}{c_l^2-c_s^2} \tag{29}$$

$$K=\rho\left(c_l^2-\frac{4}{3}c_s^2\right) \tag{30}$$

$$\nu=\frac{c_l^2-2c_s^2}{2\left(c_l^2-c_s^2\right)} \tag{31}$$

Our task now is to develop a method to calculate the density and the velocities as accurately as possible, at least enough to measure small differences in the values due to different concentrations of nanoparticles within the volume of the material

3. Method for the measurement of the parameters

3.1. Measurements of longitudinal and shear velocity

The proposed method to calculate both longitudinal and shear velocities is based on the use of simultaneous pulse-echo and through-transmission immersion ultrasonic measurements, which allow the calculation of all required parameters with high accuracy and without any prior knowledge of the material properties [2]. Fig. 2a shows the upper view of a typical immersion set-up in which the transmitter T_1 and the receiver T_2 are faced perpendicularly in opposite sides of the water basin, and the specimen in between them, which can be moved and rotated using a computer controlled $XYZ-\Phi$ scanner that allows the scanning of the specimen in all its surface as well as its rotation along the scanning axis.

The advantage of this method is that it only requires four measurements while keeping the layout of the transducers. First, the specimen (variable unknown thickness L, longitudinal velocity c_l and shear velocity c_s) is inserted between transducers at appropriate distances (d_1 and d_2). Then, transducer T_1 sends a pulse and simultaneously reflected and passed-through signals are recorded in transducer T_1 and T_2 respectively as $s_R(t)$ and $s_T(t)$ (Fig. 1a). Note that $s_R(t)$ contains reflections from front and back surfaces of the specimen, which will be later gated and separated as $s_{R1}(t)$ and $s_{R2}(t)$ respectively. Finally, the specimen is removed and transducer T_1 sends a pulse through the water-path (Fig. 2b), which is received in transducer T_2 and recorded as $s_W(t)$, which will be used as reference signal.

According to Fig. 2b, the distance between transducers T_1 and T_2 can be obtained using the time of flight of the water-path signal $s_W(t)$ without sample, t_W. Thus, assuming known the speed of sound in water c_W:

$$d_1+L+d_2=c_Wt_W \tag{32}$$

where distance d_1 and thickness L can be calculated respectively as:

$$d_1=c_Wt_{R1}/2 \tag{33}$$

and

$$L=c_L(t_{R2}-t_{R1})/2 \tag{34}$$

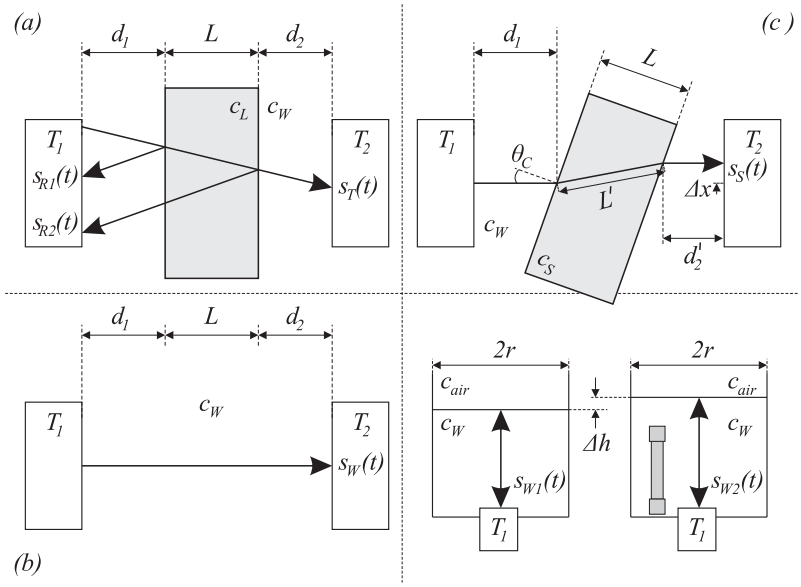

Fig. 2. Experiment set-up for (a) normal incidence (b) water-path signals (c) angular incidence (d) density measurement.

with t_{R1} and t_{R2} the times of flight of $s_{R1}(t)$ and $s_{R1}(t)$ respectively, and c_L the longitudinal velocity within the material.

On the other hand, the time of flight of the passed-through signal $s_T(t)$ with sample, t_T, will be equal to the sum of the time of flights of the different segments, thus:

$$\frac{d_1}{c_W}+\frac{L}{c_L}+\frac{d_2}{c_W}=t_T \tag{35}$$

Now, combining (32)–(35), the longitudinal sound velocity and the thickness can be calculated as:

$$c_L=c_W\left(\frac{2(t_W-t_T)}{t_{R2}-t_{R1}}+1\right) \tag{36}$$

and

$$L=\frac{c_W}{2}(2(t_{RW}-t_{RT})+(t_{R2}-t_{R1})) \tag{37}$$

Once the longitudinal velocity is known, the first critical angle can be calculated using Snell's Law and the phenomenon of mode conversion. According to this phenomenon, when the wave front passes through the interface between two media with different indexes of refraction (i.e., different velocities of the acoustic waves) at an oblique angle, part of the longitudinal wave becomes a shear wave. Snell's Law describes the relationship between angles of incidence, velocities and wave modes as shown in Fig. 3a and can be written as:

$$\frac{\sin\theta_{L1}}{c_{L1}}=\frac{\sin\theta_{L2}}{c_{L2}}=\frac{\sin\theta_{s1}}{c_{s1}}=\frac{\sin\theta_{s2}}{c_{s2}} \tag{38}$$

where c_{L1} is the longitudinal wave velocity in material 1 with θ_{L1} its angle of incidence, c_{L2} is the longitudinal wave velocity in material 2 with θ_{L2} its angle of refraction, c_{s1} is the shear wave velocity in material 1 with θ_{s1} its angle of reflection, and c_{s1} is the shear wave velocity in material 2 with θ_{s2} its angle of refraction. Note that part of the energy is reflected in medium 1 in the longitudinal mode(c'_{L1}) with reflection angle equal to the incident angle.

As can be seen in (38), when a front wave passes from a slower to a faster material, there is an incident angle that makes the refraction angle for the longitudinal wave equal to 90° degrees, thus the longitudinal wave is converted into a surface following (or creep) wave. This is called the first critical angle, θ_C, and beyond this angle only the shear mode propagates through medium 2:

$$\theta_C=arc\sin\left(\frac{C_{L1}}{C_{L2}}\right) \tag{39}$$

If the incidence angle keeps increasing, there will be an angle, called second critical angle, θ_{C2}, that makes the angle of refraction of the shear wave in medium 2 equal to 90° degrees. Beyond this angle, all of the wave energy is reflected or refracted into a surface following shear (or creep) wave.

Thus, if the sample is rotated so that the incident angle lays between the first and second critical angles (Fig. 2c), only shear waves propagates through the material. This shear wave is converted back into longitudinal when the wave reaches the opposite surface of the sample, i.e. the back-face solid-water interfaces, and propagates into the water reaching the receiver. Therefore, following the setup used for the longitudinal waves but rotating the sample certain incidence angle θ_i, so that $\theta_C<\theta_i<\theta_{C2}$, if transducer T_1 sends a pulse the recorded signal $s_S(t)$ in transducer T_2 will have propagated d_1 and d_2' in water in longitudinal mode, and distance L' within the material in shear wave mode, and therefore traveling

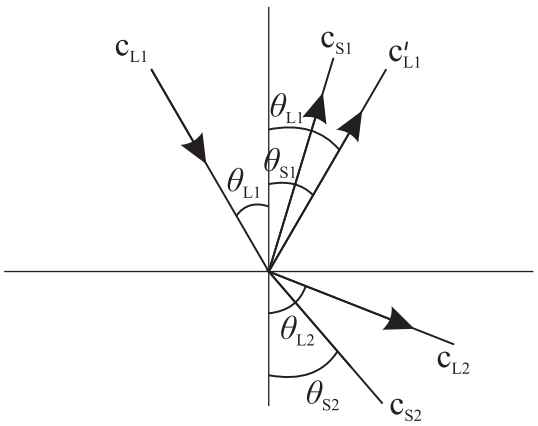

Fig. 3. Graphic examples of Snells' law.

at the shear velocity c_S in the material. Thus, (35) can be rewritten in this case as:

$$\frac{d_1}{c_W}+\frac{L'}{c_S}+\frac{d_2'}{c_W}=t_T \tag{40}$$

with t_S the time of flight of $s_S(t)$. Note that, if the incidence point in the front surface has not changed, the distances traveled now by the different waves can be derived from the geometry in Fig. 2c as:

$$L'=\frac{L}{\cos\theta_S} \tag{41}$$

and

$$d_2'=d_2-d+L'\cos(\theta_i-\theta_S) \tag{42}$$

where θ_S is the refraction angle of $s_S(t)$ than can be expressed as a function the incident angle θ_i using the Snells Law given in (38) and the shear velocity c_S as:

$$\frac{\sin\theta_i}{c_W}=\frac{\sin\theta_S}{c_S} \tag{43}$$

Finally, combining the previous equations, the shear velocity can be expressed as:

$$c_S=\frac{c_W}{\sqrt{\sin^2\theta_i+\left[\frac{c_W\cdot(t_W-t_S)}{L}+\cos\theta_i\right]^2}} \tag{44}$$

Note that the incidence point in transducer T_2 has changed the geometry of the waves, changing the trajectory of the wave certain distance (Δx in Fig. 2c), but if T_2 is an unfocused transducer and this displacement is much smaller than the transducer diameter, the resulting change does not affect the calculation of time of flight.

The method used for the calculation of the times of flight was introduced by the authors in [19]. It is based on the use of iterative deconvolution and allows to calculate all the parameters without any prior knowledge of the sample and does not need any correction from the user. It uses a reference signal extracted from a single pulse to automatically subtract the successive echoes, calculating the time of flight of the pulses using cross-correlation and sub-sample shifting in frequency domain, which, combined with cosine interpolation, allows a resolution in the measurements in the order of cm/s, which translated to the elastic constants will allow to measure slight changes in the different variables due to changes in the properties of the composites. For a more detailed information about the method for the calculation of the velocities, we encourage readers to review reference [19].

3.2. Measurement of density

For the measurement of the density we will follow two different approaches. On the one hand, it is well known that for any given solid, the density ρ can be calculated as the ratio between the acoustic impedance Z_M of the material and the longitudinal sound velocity c_L in normal incidence:

$$\rho=\frac{Z_M}{c_L} \tag{45}$$

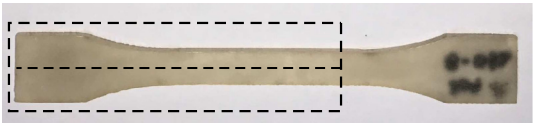

Fig. 4. Example of a specimen and the scanning area.

The acoustic impedance of the material can be calculated indirectly using the amplitude of the first echo of the reflected signal as follows. The reflection coefficient R_{WS} between the water and the material can be written as a function of their respective acoustic impedances Z_M and Z_W as:

$$R_{WS}=\frac{Z_M-Z_W}{Z_M+Z_W} \tag{46}$$

On the other hand, the reflection coefficient can also be written as the ratio between the incident and the reflected signals:

$$R_{WS}=\frac{A_{R1}}{A_{Ref}} \tag{47}$$

where A_{Ref} is the amplitude of the incident wave and A_{R1} is the peak value of the first reflection in the pulse echo signal, $s_{R1}(t)$. The density can finally be written as a function of the previous using (45)–(47) as:

$$\rho=\frac{Z_W}{c_L}\left(\frac{A_{Ref}+A_{R1}}{A_{Ref}-A_{R1}}\right) \tag{48}$$

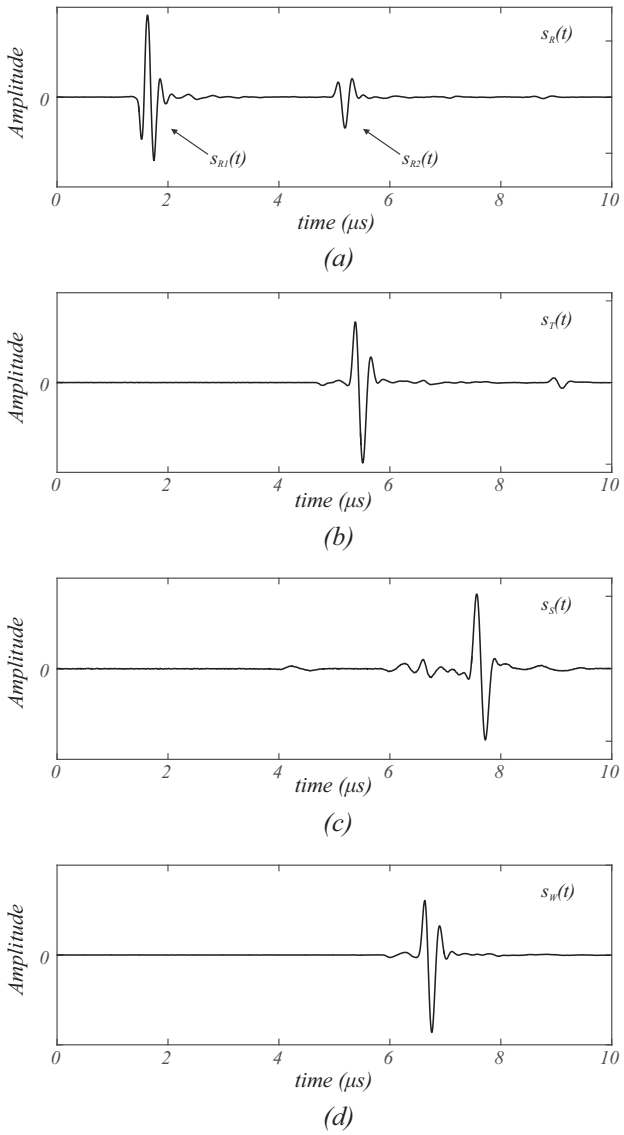

Fig. 5. Examples of Ascans (a) Pulse-echo at normal incidence (b) Through-Transmission at normal incidence (c) Through-Transmission at angular incidence (d) water-path without sample.

where c_L is calculated in the previous section, A_{R1} is the peak of the first echo received in the pulse-echo transducer, and working in a 25 °C controlled temperature environment, the acoustic impedance of the distilled water used in the experiments is also known with a constant value of $Z_W = 1.48$ MNs/m. Therefore, the only remaining incognito in (48) is the peak amplitude of the incident wave A_{Ref}.

To calculate the incident amplitude we proceed in the same way as we did for the reflected wave, but in this case the material is substituted by air, and signal acquired in transducer T_1 is now called $s_{Ref}(t)$ whose peak amplitude is A_{Ref}. Taking into account that the acoustic impedance of air is much smaller than that of water ($Z_W = 1,480,000$ N s/m $\gg 413.3$ N s/m $= Z_{Air}$), the reflection coefficient between them is close to 1 (in magnitude), so all the energy is reflected back to the transducer, therefore the received echo is the incident wave at the water surface distance.

According to the previous, if the material is then placed at exactly the same distance from the transducer as it was from the water surface (d_1 in Fig. 2a), the ratio between the reflections will provide the desired reflection coefficient between the water and the material that can be used in (48) to calculate the density. It must be taken into account that, using focused transducers, as both signals have traveled the same distance and have hit the corresponding surface at the same place, the diffraction effects are negligible. The second method proposed is based on the Archimedean method. Density can be measured as a function of the mass (m) and volume (V) of the material as:

$$\rho = \frac{m}{V} \tag{49}$$

The mass can be measured using a precision balance, and the volume can be calculated using ultrasound as follows. As shown in Fig. 2d, the focused ultrasonic transducer T_1 is placed at the bottom of a cylindrical water basin of known diameter, and an ultrasonic pulse is send towards the surface of the interface water/air, recording the signal as $s_{W1}(t)$. Then, the sample is introduced in the basin and, once the surface of the interface has stabilized, another pulse is sent to the interface recording the signal as $s_{W2}(t)$. Therefore, assuming known the speed of sound in water

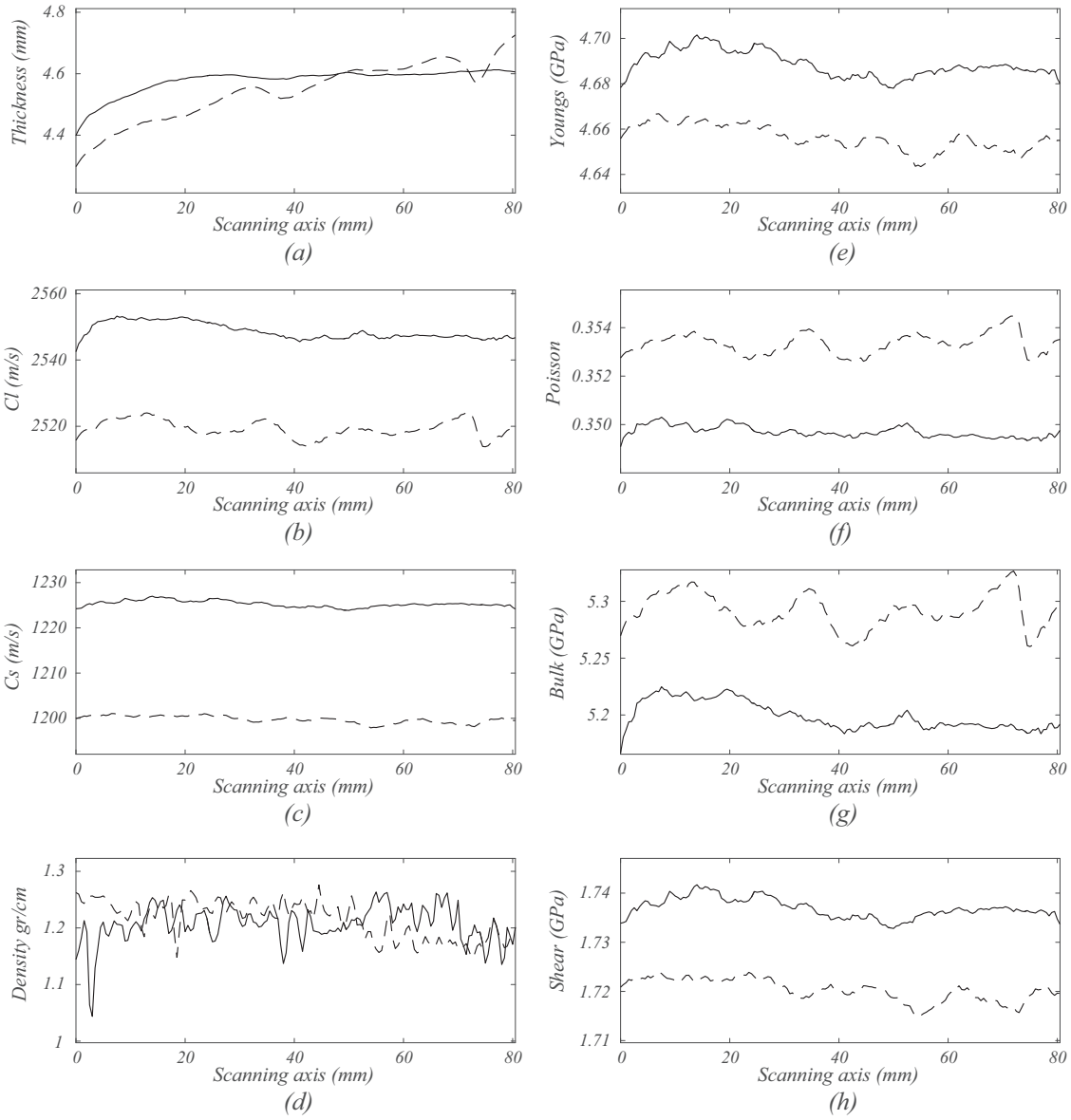

Fig. 6. Profiles of the results obtained for a sample of series B (solid line) and A4 (dashed line) for (a) thickness (b) longitudinal velocity (c) shear velocity (d) density (e) Young's modulus (f) Poisson ratio (g) Bulk modulus and (h) shear modulus.

c_W, the difference in the height of the water column with and without sample can be calculated using the time of flight between pulses $s_{W1}(t)$ (t) and $s_{W2}(t)$, as:

$$\Delta h = c_W \cdot (t_{W2} - t_{W1}) \tag{50}$$

Now, the volume of the sample can be calculated as the volume of the displaced cylindrical column of water as:

$$V = \pi r^2 \cdot \Delta h \tag{51}$$

where r is the radius of the cylinder. Finally, the density is expressed as a function of the time of flights and sound velocity in water as:

$$\rho = \frac{m}{\pi r^2 \cdot \Delta h \cdot c_W \cdot (t_{W2} - t_{W1})} \tag{52}$$

4. Experiments and results

4.1. Experimental setup

In order to obtain the desired parameters, an experimental ultrasonic setup was designed according to Fig. 2, in which the transmitter T_1 was a 5 MHz wide band focused transducer IRY405 from NDT Transducers LLC and receiver T_2 was a composite 5 MHz transducer TF5C6 from Doppler Electronic Technologies. The liquid used was distilled water and temperature was controlled to be at 25 °C during all the experiment. The movement of the samples for the 2D scan was made with a 3D scanner designed for that purpose synchronized with the pulser, together with a precision step motor for the rotation of the samples, controlled also by the scanning software. The resolution in the XY axes was 200 μm per step, 100 μm in the Z axis and 1.8° in the angular axis. The pulser receiver used was a SE-TX06-00, with sampling frequency of the acquisition system set to 100 MHz and sampling windows length adjusted in order to have all measurements of each experiment in the same time basis. A 100 ns 5 MHz pulse was used as excitation.

The equipment used for the destructive tensile testing for the comparison was a Zwick ProLine Z100 with control software Xpert. The separation between jaws was 115 mm, and the misalignment of the test pieces was controlled by gauges incorporated in the clamps. The pre-tension introduced in the jaw clamp was removed by the software. A pre-load of 0.1 MPa was applied to eliminate the initial jaw tightening error in the stress–strain curve. The modulus of elasticity was calculated according to ISO 527-1:2012 by means of a regression line of the values obtained by the extensiometric gauge in stretch steps of 0.05, with a test speed of 1 mm/min.

The specimens used for the analysis were samples of a polyester resin from GAZECHIM doped with different concentrations of graphene nanoparticles. Specimen series B is the control specimen without any nanoparticles, and specimen series A1–A4 were produced with increasing, but very small, different concentrations of graphene nanoparticles. 8 specimens were analyzed for each series, resulting in 40 specimens analyzed. The particular values of the graphene concentrations are not provided as they are protected under nondisclosure agreements, but note that the aim of this work is to analyze the ability of the proposed system on the analysis of the dispersion within the specimens, thus the particular composition of the samples is not required. The specimens were made according to EN ISO 527-4 using a silicone matrix according to the casting procedure. After the curing process, the specimens were introduced into a martyr and machined to a target thickness of ≈ 4 mm. Fig. 4 shows one of the samples that has been analyzed.

For each specimen, 80 mm were analyzed along its longitudinal axis (see dashed line in Fig. 4) in steps of 0.5 mm to obtain a Bscan of all the parameters, resulting in 160 measurements for each spec-

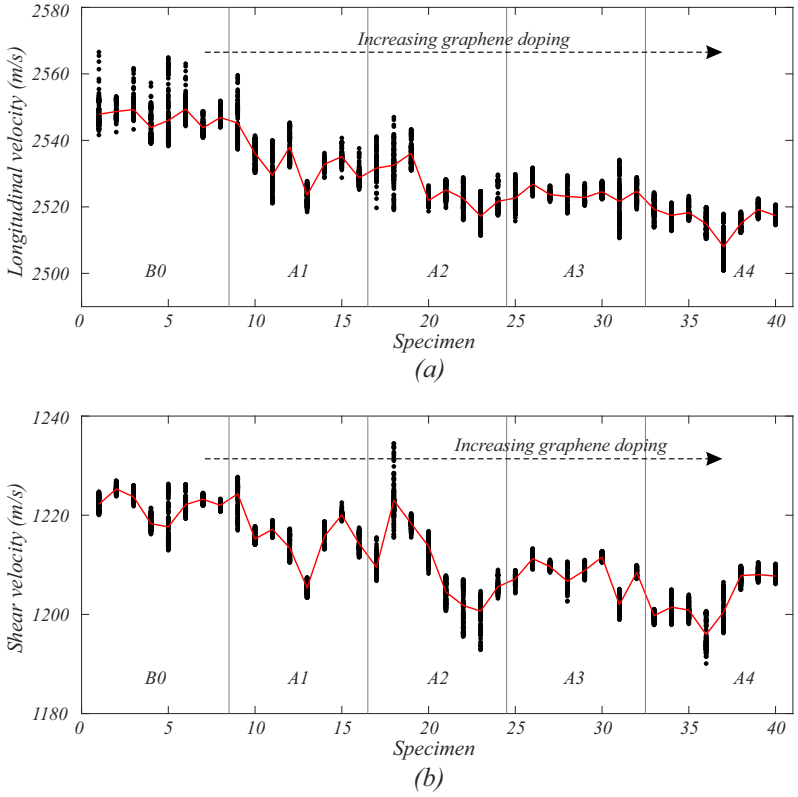

Fig. 7. Dispersion of velocities for each specimen (dots) and velocities' trends (red lines) for (a) longitudinal velocity and (b) shear velocity. (For interpretation of the references to color in this figure legend, the reader is referred to the web version of this article.)

imen. At each point, 25 Ascans were acquired and averaged to reduce the noise. Note that each specimen is first scanned with its faces perpendicular to the transducers, then rotated certain angle with the precision step motor and scanned again to measure the signals required to get the shear velocity. All the procedure is done automatically, so no action is required for the user besides changing the specimen once the scanning is done. The first and second critical angles were estimated using the standard longitudinal velocity provided by the manufacturer, ≈ 2600 m/s, and were later verified with experimental data. Therefore, using Snell's Law and assuming that typical shear velocity should be around half the longitudinal velocity, the first and second critical angles lay around 35° and 60°, thus an angle of 50.4° was chosen as incident angle for the shear wave experiment.

The amplitude used as reference for the acoustic impedance measurements was obtained with a water column using a cylindrical water basin with the transducer attached to the bottom and controlling the temperature of the water to the standard 25 °C used for the whole experiment. The same focused transducer was used to acquire the signal, setting the column of water to 3.8 mm (nominal focal distance of the transducer) and acquiring 100 samples that were averaged in order to reduce the noise and to average surface unevenness. This very same distance was used to place the samples for their scanning, so that the front face of the samples were at 3.8 mm of the transducer T_1. After measuring the water interface signal, samples were immersed in the water column for the volume measurement repeating the previous procedure. The balance used to weight the samples for the density measurements was a precision balance KERN PLT from KERNEL.

4.2. Results

Fig. 5 shows an example of the different Ascans used for the calculations. As aforementioned, it is required to have the time of flight between first and second echo in transducer T_1 (Fig. 5a), the time of flight between through-transmission signal at normal incidence (Fig. 5b) and water-path signal (Fig. 5d), and the time of flight between through-transmission signal at 50.5° rotation (Fig. 5c) and water-path signal (Fig. 5d). Signals have been normalized in the graphics for a better appreciation of the time difference between them.

Once the algorithm is fed with the corresponding signals from the Bscan of each specimen, the required parameters can be calculated. Fig. 6 shows the results obtained for one of the control specimens (series B, solid line in the figure) compared with those obtained from a specimen with a significant amount of nanoparticles (series A4, dashed line in the figure).

As can be seen in Fig. 6b and c, values of velocities are very homogeneous for the control specimen, as expected (standard deviation of 2.43 m/s and 0.58 m/s for the longitudinal and shear velocities respectively), as it is free of nanoparticles and supposed to be homogeneous. On the other hand, the doped composite presents also a homogeneous dispersion of the nanoparticles within the sample (standard deviation of 2.56 m/s and 0.71 m/s for the longitudinal and shear velocities respectively). For both specimens, this behavior is translated to the profiles of the elastic constants (Fig. 6e, f, g and h). Anyhow, even for the doped specimen in which there is a slight deviation (see for example Bulk modulus in Fig. 6g.), the dispersion is very small, which is an indication of the suitability of the method followed for the mixing.

Unfortunately, results for the density measurements are not that good. They show a high dispersion even for the control undoped specimen, which is an indication of the failure of the procedure. It is mainly due to the unevenness of the surface of the specimen. Note that, as described in the previous section, calculation of the density requires the correct measurement of the amplitude of the signals at normal incidence, and deviation from normality results in a strong deviation from the correct acoustic impedance value. Normal incidence is easy to achieve for the water surface, but due to the sample bending during curing and surface irregularities after polishing, the values obtained are unreliable. Therefore, for the calculation of the elastic constant we have decided to use the global Archimedean densities which are very reliable and accurate.

Continuing with our analysis, next figure shows the values of longitudinal (Fig. 7a) and shear (Fig. 7b) velocity obtained for all specimens, where the trend and dispersion of the values can be clearly seen. Black dots represent the values of the velocities, and the red line connect the average of each specimen.

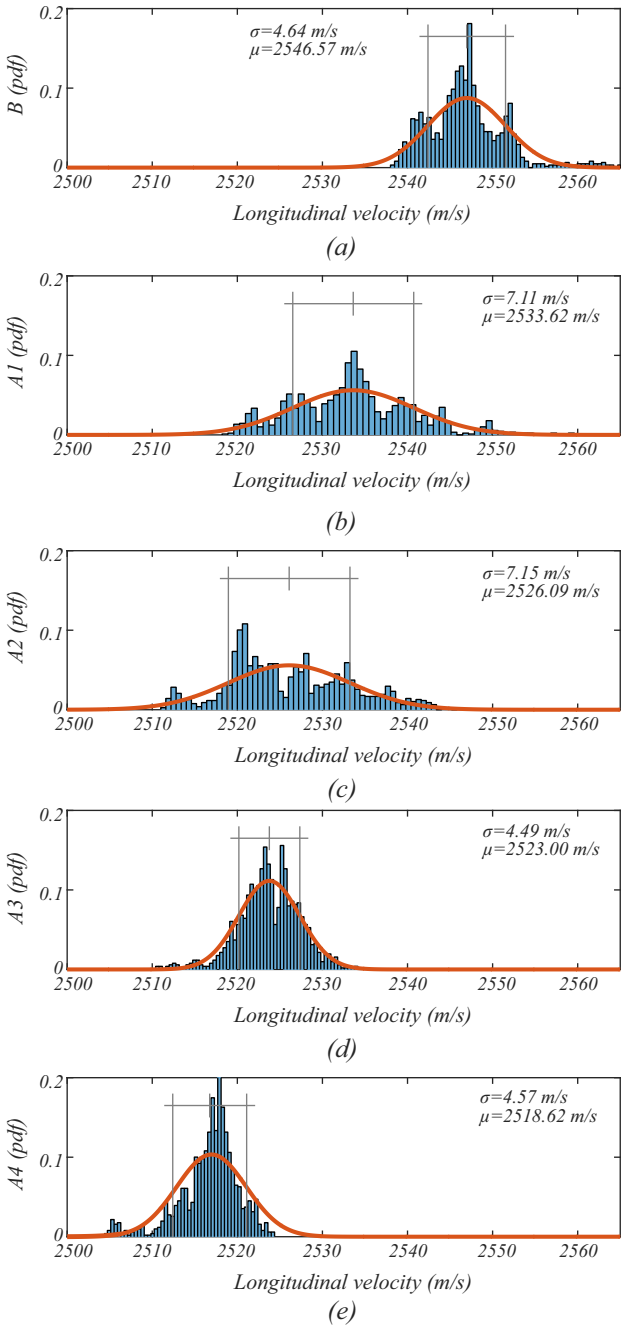

Fig. 8. Histograms of the longitudinal velocities for each series with its fitted Gaussian PDF (red lines) (a) B0 (b) A1 (c) A2 (d) A3 and (e) A4. (For interpretation of the references to color in this figure legend, the reader is referred to the web version of this article.)

Fig. 7 shows the influence of the proportion of nanoparticles in the velocity, as we can see that the higher the amount of nanoparticles, the lower the velocity both for longitudinal and shear waves. For a better analysis of the dispersion in the results, Fig. 8 shows the histogram of the longitudinal velocities for each series, in which its fitted Gaussian probability density function (PDF) is superimposed to the bins, with their corresponding mean and standard deviation. Note that in all cases the standard deviation is around the 0.5% of the value of the mean velocity, which is a very good indication in terms of homogeneity. Anyhow, it seems that the higher the amount of dopant, the lower the standard deviation, which suggest that including certain amount of dopant in the dissolution stabilizes somehow the samples. Tables 1 and 2 summarizes the mean results obtained for all the parameters for each series.

This homogeneity in the results is translated to all the parameters. Fig. 9 shows the resulting trends of all the parameters considering the averaged values of all the specimens in each series. As can be seen, velocities decrease as the amount of graphene increases (Fig. 9a and b). Concerning the elastic constants, the decrement in the velocities causes a decrease in the Young's and Shear modulus and an increment in the Bulk modulus and the Poisson's ratio for the specimens with the lowest concentration of graphene (A1 and A2). However, there is an inflexion point beyond which the increment in the concentration increases the density considerably (Fig. 9d), reverting the trend of the elastic constants, as can be seen in Fig. 9c for the Youngs Modulus.

Fig. 10 shows the results obtained for the Youngs modulus with the destructive tensile test. As can be seen, the trends are exactly the same, despite the difference in the magnitude due to the differ-

Table 1
Resume of mean and standard deviation (std) obtained for density and velocities for each series.

Specimen	Density		Longitudinal velocity		Shear velocity	
	Mean (kg/m)	Std (g/cm)	Mean (m/s)	Std (m/s)	Mean (m/s)	Std (m/s)
B0	1.175	11.27	2546.57	4.64	1221.97	3.02
A1	1.168	7.09	2533.62	7.11	1215.69	5.37
A2	1.167	12.95	2526.09	7.15	1209.64	7.98
A3	1.173	13.84	2523.00	4.49	1208.20	3.13
A4	1.187	26.37	2518.06	4.57	1202.80	3.72

Table 2
Resume of mean and standard deviation (std) obtained for Young's modulus and Poisson ratio for each series.

Specimen	Young's M.		Poisson	
	Mean (GPa)	Std (Mpa)	Mean	Std
B0	4.740	47.65	0.3504	0.0008
A1	4.664	59.24	0.3505	0.0012
A2	4.616	63.39	0.3512	0.0020
A3	4.627	44.99	0.3512	0.0006
A4	4.643	46.71	0.3522	0.0007

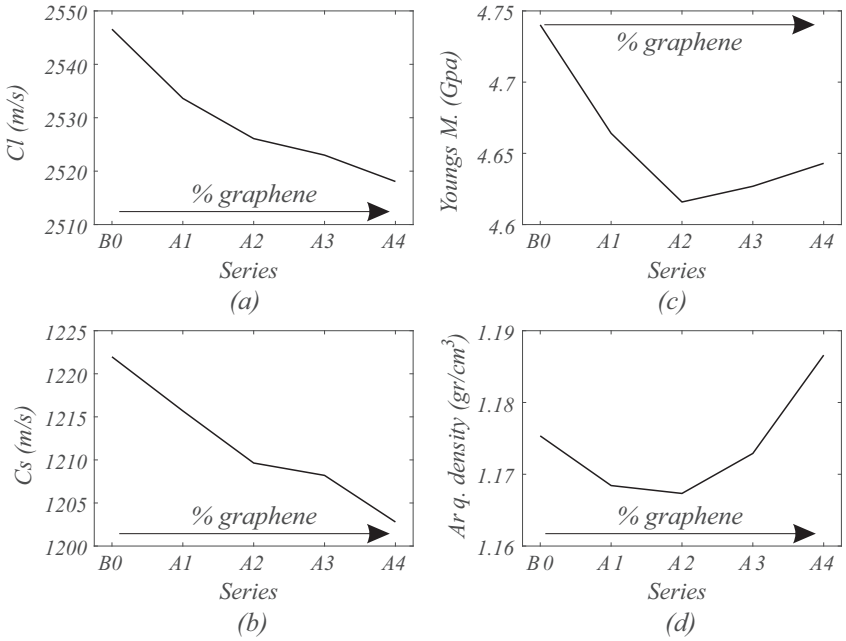

Fig. 9. Mean trends for (a) longitudinal velocity (b) shear velocity (c) Young's Modulus and (d) density.

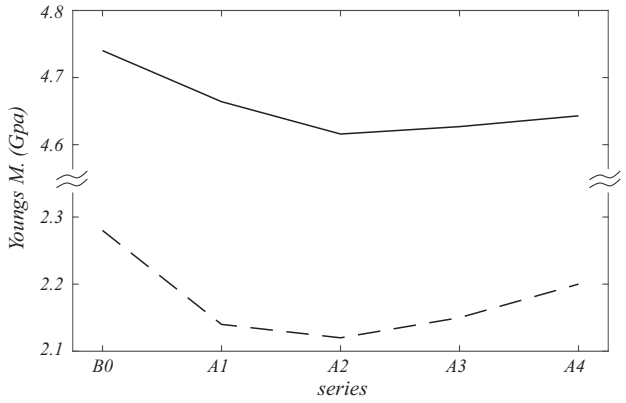

Fig. 10. Comparison of the mean Young's Modulus for each series for (a) ultrasonic test and (b) tensile stress test.

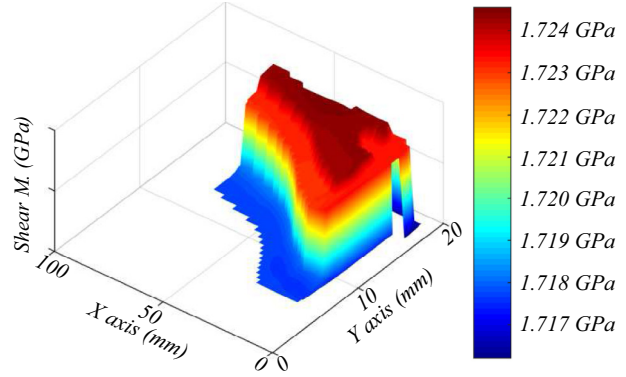

Fig. 11. Example of 3D analysis of the Bulk modulus for an A3 series sample. Area analyzed showed as dashed rectangle in Fig. 4.

ence in the nature of the forces analyzed with each technique. From many observations it is known that the elastic parameters obtained from so called static laboratory tensile test differ from those obtained by inverting the wave velocities. The discrepancy between the "static" and "ultrasonic dynamic" moduli of samples has been reported to be on the order of 20% for solids and $> 40\%$ for some viscoelastic materials, whereby ultrasonic dynamic moduli are usually higher than static [33,35,36].

Finally, Fig. 11 shows an example of a 3D scanning of one sample of the A3 series for the Bulk modulus, which is a good example of the possibilities of the method to provide information about the dispersion of the elastic properties in the sample.

5. Conclusions

In this work we have presented a method for the mechanical characterization of nanoparticles doped composites using ultrasound. It calculates the elastic constants through the longitudinal and shear sound velocities and the local density, acquired using an immersion ultrasonic set-up and an automatic iterative deconvolution algorithm. The set-up is quite simple an inexpensive, and can be used in the manufacturers laboratory to control the resins and nanoparticles mixing results in small samples.

The accuracy and precision achieved in the velocity measurements is translated to the calculated elastic constants, revealing small changes in the local distribution of nanoparticles, which can be used as an indication of success in the mixing procedure. We have tested the method using real samples of a polyester resin doped with different small amounts of graphene nanoparticles, and the method has been able to differentiate the changes in the elastic constants due do the changing amount of dopant. It also has shown that the method used for the mixing is appropriate, as the dispersion found within the samples is very small.

On the other hand, the proposed method for the estimation of the local density within the samples, although the average values measured for each sample are close to the standard Archimedean values, has shown to be very sensitive to surface unevenness and bending, resulting in unreliable and very disperse values, thus it cannot be used instead of Archimedean measures. For future experiments, we will use semi-closed matrices to force flatness in the surfaces of the samples.

Finally,the trends in the different parameters are in good agreement with the elastic constants obtained with standard tensile test, which is a good indicator of the performance of the method. On the other hand, static (tensile test) and ultrasonic "dynamic" values obtained for the Young's modulus, although correlated, show a significant bias (around 50% in the worst case) due to the viscoelastic behavior of the resins. One of the next steps of the work will be to analyze this discordance to find a relation between these two set of measures, which will allow to estimate the tensile test results of new products under development before their destructive testing, which is costly and time consuming. The set-up and the method described in this work are actually being used in a graphene manufactures' laboratory to control the resins doping and nanoparticles functionalization, and is now being adapted to be able to perform similar measurements but for anisotropic structures, so it can be used for the characterization of fiber-reinforced composites doped with nanoparticles.

Acknowledgment

This research was partially funded by a grant (DPI2016-78876-R-AEI/FEDER, UE) from the Spanish State Research Agency (AEI) and the European Regional Development Fund (ERDF/ FEDER)

References

[1] E. Manias, Nanocomposites: stiffer by design, Nat. Mater. 6 (1) (2007) 9–11, http://dx.doi.org/10.1038/nmat1812.
[2] G.N. Greaves, A.L. Greer, R.S. Lakes, T. Rouxel, Poissons ratio and modern materials, Nat. Mater. 10 (2011) 823–837, http://dx.doi.org/10.1038/nmat3134.
[3] Q.G. Chi, J.F. Dong, C.H. Zhang, C.P. Wong, X. Wand, Q.Q. Lei, Nano iron oxide-deposited calcium copper titanate/polyimide hybrid films induced by an external magnetic field: toward a high dielectric constant and suppressed loss, J. Mater. Chem. C 4 (2016) 8179–8188, http://dx.doi.org/10.1039/C6TC01655C.
[4] Y. Wu, J. Hu, C. Zhang, J. Han, Y. Wang, B. Kumar, A facile approach to fabricate a uv/heat dual-responsive triple shape memory polymer, J. Mater. Chem. A 3 (2015) 97–100, http://dx.doi.org/10.1039/C4TA04881D.
[5] Q. Chi, J. Sun, C. Zhang, G. Liu, J. Lin, Y. Wang, X. Wang, Q. Lei, Enhanced dielectric performance of amorphous calcium copper titanate/polyimide hybrid film, J. Mater. Chem. C 2 (2014) 172–177, http://dx.doi.org/10.1039/C3TC31757A.
[6] A. Gedaken, Doping nanoparticles into polymers and ceramics using ultrasound radiation, Ultrason. Sonochem. 14 (4) (2006) 418–430, http://dx.doi.org/10.1016/j.ultsonch.2006.08.005.
[7] J.N. Coleman, U. Khan, Y.K. Gun'ko, Mechanical reinforcement of polymers using carbon nanotubes, Adv. Mater. 18 (6) (2006) 689–706, http://dx.doi.org/10.1002/adma.200501851.
[8] J.N. Coleman, U. Khan, W.J. Blau, Y.K. Gunko, Small but strong: a review of the mechanical properties of carbon nanotube polymer composites, Carbon 44 (9) (2006) 1624–1652, http://dx.doi.org/10.1016/j.carbon.2006.02.038.
[9] D. Gersappe, Molecular mechanisms of failure in polymer nanocomposites, Phys. Rev. Lett. 89 (2002) 058301, http://dx.doi.org/10.1103/PhysRevLett.89.058301.
[10] T. Uygunoglua, I. Gunes, W. Brostow, Physical and mechanical properties of polymer composites with high content of wastes including boron, Mater. Res. 18 (6) (2015) 1188–1196, http://dx.doi.org/10.1590/1516-1439.009815.
[11] H. Hu, L. Zhao, J. Liu, Y. Liu, J. Cheng, J. Luo, Y. Liang, Y. Tao, X. Wang, J. Zhao, Enhanced dispersion of carbon nanotube in silicone rubber assisted by graphene, Polymer 53 (2012) 3378–3385, http://dx.doi.org/10.1016/j.polymer.2012.05.039.

[12] R. Ramanathan, A.A. Abdala, S. Stankovich, D.A. Dikin, M. Herrera-Alonso, R.D. Piner, D.H. Adamson, H.C. Schniepp, X. Chen, R.S. Ruoff, S.T. Nguyen, I.A. Aksay, R.K. PrudHomme, L.C. Brinson, Functionalized graphene sheets for polymer nanocomposites, Nat. Technol. 3 (2008) 327–331, http://dx.doi.org/10.1038/nnano.2008.96.
[13] D.L. Ciprari, Mechanical Characterization of Polymer Nanocomposites and The Role of the Interphase, Master's thesis, Georgia Institute of Technology.
[14] P. Song, L. Liu, G. Huang, Y. Yu, Q. Guo, Largely enhanced thermal and mechanical properties of polymer nanocomposites via incorporating c60@graphene nanocarbon hybrid, Nanotechnology 24 (50). http://dx.doi.org/10.1088/0957-4484/24/50/505706.
[15] X. Zhao, Q. Zhang, D. Chen, Enhanced mechanical properties of graphene-based poly(vinyl alcohol) composites, Macromolecules 43 (2010), http://dx.doi.org/10.1021/ma902862u, 2375–2365.
[16] W. Michaeli, U. Klemradt, A. Elas, K. Berdel, D. Carmele, Evaluating dispersion in nanocomposites, Plast. Res. Online. http://dx.doi.org/10.2417/spepro.000050.
[17] S.M.L. Silva, C.R.C. Braga, M.V.L. Fook, C.M.O. Raposo, L.H. Carvalho, E.L. Canedo, Application of Infrared Spectroscopy to Analysis of Chitosan/Clay Nanocomposites, InTech, 2012, pp. 44–62 (Chapter Infrared Spectroscopy – Materials Science, Engineering and Technology).
[18] P. He, J. Zheng, Acoustic dispersion and attenuation measurement using both transmitted and reflected pulses, Ultrasonics 39 (1) (2001) 27–32, http://dx.doi.org/10.1016/S0041-624X(00)00037-8.
[19] A. Rodríguez, L. Svilainis, V. Dumbrava, A. Chaziachmetovas, A. Salazar, Automatic simultaneous measurement of phase velocity and thickness in composite plates using iterative deconvolution, NDT&E Int. 66 (2014) 117–127, http://dx.doi.org/10.1016/j.ndteint.2014.06.001.
[20] L. Svilainis, A. Rodríguez, V. Dumbrava, A. Chaziachmetovas, V. Eidukynas, Estimation of composite plate attenuation, Elektron. Elektrotechnika 20 (1) (2014) 59–62, http://dx.doi.org/10.5755/j01.eee.20.1.4675.
[21] R. Asher, Ultrasonics in chemical analysis, Ultrasonics 25 (1) (1987) 17–19, http://dx.doi.org/10.1016/0041-624X(87)90004-7.
[22] J.M. Hale, Ultrasonic density measurement for process control, Ultrasonics 26 (6) (1988) 356–357, http://dx.doi.org/10.1016/0041-624X(88)90036-4.
[23] R.T. Higuti, J.C. Adamowski, Ultrasonic densitometer using a multiple reflection technique, IEEE Trans. Ultrason. Ferroelectr. Freq. Contr. 49 (9) (2002) 1260–1268, http://dx.doi.org/10.1109/TUFFC.2002.1041543.
[24] S. Hoche, M.A. Hussein, T. Becker, Ultrasound-based density determination via buffer rod techniques: a review, Sens. Sens. Syst. 2 (2013) 103–125, http://dx.doi.org/10.5194/jsss-2-103-2013.
[25] S. Hoche, M.A. Hussein, T. Becker, Density, ultrasound velocity, acoustic impedance, reflection and absorption coefficient determination of liquids via multiple reflection method, Ultrasonics 57 (2015) 65–71, http://dx.doi.org/10.1016/j.ultras.2014.10.017.
[26] R. Hill, Elastic properties of reinforced solids: some theoretical principles, J. Mech. Phys. Solids 11 (5) (1963) 357–372, http://dx.doi.org/10.1016/0022-5096(63)90036-X.
[27] D.R. Askeland, P.P. Phulé, The Science and Engineering Materials, first ed., Thompson Learning.
[28] A. Kaselow, The Stress Sensitivity Approach: Theory and Application, Ph.D. thesis, Institute of Geological Sciences, Berlin, Freie Univ.
[29] S.S. Reddy, K. Balasubramaniam, C.V. Krishnamurthy, M. Shankar, Ultrasonic goniometry immersion techniques for the measurement of elastic moduli, Compos. Struct. 61 (1) (2005) 3–17, http://dx.doi.org/10.1016/j.compstruct.2004.01.008.
[30] B.A. Auld, Acoustic Fields and Waves in Solids, vol. 1., second ed., John Wiley.
[31] K.P. Menrad, Dynamic Mechanical Analysis. A Practical Introduction, first ed., CRC Press.
[32] J.W. Littles, L.J. JAcobs, A.H. Zureick, Review of Progress in Quantitative Nondestructive Evaluation, vol. 16, Plenum Press, 1997, pp. 1807–1814 (Chapter The ultrasonic measurement of elastic constants of structural FRP composites).
[33] J. Vincent, Structural Biomaterials, 3rd Edition, Princeton University Press.
[34] V. Grechka, A. Pech, I. Tsvankin, B. Han, Velocity analysis for tilted transversely isotropic media: a physical modeling example, Geophysics 66 (3) (2001) 904–910, http://dx.doi.org/10.1190/1.1444980.
[35] R.E. Smith, Ultrasonic elastic constants of carbon fibers and their composites, J. Appl. Phys. 43 (6) (1972) 2555–2561, http://dx.doi.org/10.1063/1.1661559.
[36] A.N. Tutuncu, M.M. Sharma, Relating static and ultrasonic laboratory measurements to acoustic log measurements in tight gas sands, in: SPE Annual Technical Conference and Exhibition. http://dx.doi.org/10.2118/24689-MS.